2015

The Inhibitory Effects of Opioids on Voltage-gated Calcium Influx in Neonatal Rat Carotid Body Type I Cells

Ellen M. Ricker
Wright State University

THE INHIBITORY EFFECTS OF OPIOIDS ON VOLTAGE-GATED CALCIUM INFLUX IN NEONATAL RAT CAROTID BODY TYPE I CELLS

A thesis submitted in partial fulfillment
of the requirement for the degree of
Master of Science

By

ELLEN MARIE RICKER
B.S., University of Dayton, 2012

2015
Wright State University

WRIGHT STATE UNIVERSITY

GRADUATE SCHOOL

1/24/2014

I HEREBY RECOMMEND THAT THE THESIS PREPARED UNDER MY SUPERVISION BY Ellen Marie Ricker ENTITLED The Inhibitory Effects of Opioids on Voltage-gated Calcium Influx in Neonatal Rat Carotid Body Type I Cells BE ACCEPTED IN PARTIAL FULFILLMENT OF THE REQUIREMENT FOR THE DEGREE OF Master of Science.

Christopher Wyatt, Ph.D.
Thesis Director

Timothy Cope, Ph.D.
Department Chair
Department of Neuroscience, Cell Biology and Physiology

Robert E. W. Fyffe, Ph.D.
Vice President for Research and
Dean of the Graduate School

Committee on
Final Examination

Debra Mayes, Ph.D.

David Ladle, Ph.D.

ABSTRACT

Ricker, Ellen Marie. M.S., Department of Neuroscience, Cell Biology, and Physiology, Wright State University, 2015. The inhibitory effects of opioids on voltage-gated calcium influx in neonatal rat carotid body type I cells.

It is known that opioids inhibit the hypoxic ventilatory response, but little is known about the mechanisms that underpin this. This study's objectives were to examine which opioid receptors are located on the oxygen-sensing carotid body type I cells and determine whether selective agonists inhibit cellular excitability.

Immunocytochemistry revealed the presence of μ and κ opioid receptors on type I cells. The μ-selective agonist DAMGO (10μM) and the κ-selective agonist U50-488 (10μM) significantly ($p<0.0025$ and $p<0.0095$ respectively, unpaired student's t-test) inhibited high K^+ induced rises in intracellular Ca^{2+} compared with controls. After a three-hour incubation with pertussis toxin, a G_i protein-coupled inhibitor, DAMGO and U50-488 (10μM) has no significant effect on the responses to K^+.

These results indicate that opioids acting at μ and κ receptors inhibit voltage-gated Ca^{2+} influx in carotid body type I cells. This mechanism may explain, in part, why opioids inhibit the hypoxic ventilatory response.

This work appeared in abstract form at the Ohio Physiological Society meeting 2013.

TABLE OF CONTENTS

LIST OF FIGURES

TABLES

Table Page

ACKNOWLEDGEMENTS

There are several people that I would like to thank who have made this project possible. First and foremost, I would like to thank Dr. Wyatt for welcoming me into his lab, for sharing his passion of the carotid body and a few beers, and most of all, for teaching me the superstitions behind science. Secondly, I would like to thank the members of the Wyatt Lab. Thanks to Barbara Barr for teaching me the necessary protocols and always warning me when a storm is coming. Also, many thanks to Richard Pye, who, among many other things, has been a guiding light by fully convincing me to not pursue a Ph.D.

Thank you also to Paula Bubulya, who allowed access to her Deltavision microscope necessary for immunohistochemistry. Thank you to my committee members, Dr. Mayes and Dr. Ladle, for their help in improving this thesis. Thank you to the Neuroscience, Cell Biology, and Physiology Department and the Anatomy Master's Program for the opportunity to conduct research. A special thank you to Marc Thoma, who only fell asleep once while listening to my presentations countless times. And finally, thank you to my supportive family, who even though they may not fully understand this work, admire my colorful figures.

For my parents.

INTRODUCTION

THE CAROTID BODY

The carotid bodies (CB) are sensory organs that sit bilaterally at the bifurcation of the common carotid arteries in the neck (Figure 1A). These small organs are the body's primary peripheral chemoreceptors meaning they modulate breathing in response to changes in arterial gases and pH. In response to hypoxia, hypercapnia, and acidosis, the carotid bodies release neurotransmitters that can culminate in hyperventilation to restore blood gas homeostasis.

Microanatomy of the Carotid Body

There are two main types of cells that make up the CB: type I cells and type II cells (Figure 1B). Forming the majority of the organ, type I, or glomus cells, are the excitable cells responsible for forming synapses with afferents from the carotid sinus nerve (CSN). Type I cells are distinguished by their large, dense-core vesicles, that contain neurotransmitters which are important in the acute hypoxic ventilatory response (Gonzalez *et al*, 1994). Between adjacent type I cells, gap junctions allow the cells to communicate with each other, while tight junctions hold the cells in a glomerulus (Gonzalez *et al.*, 1994; Kumar & Prabhakar, 2012). Where type I cells are not joined with one another, type II, or sustentacular cells act like glia to hold the CB together. Type II cells account for less than 20% of the organ (De Kock, 1966), and unlike type I cells, type II cells are not excitable and do not form synapses with the CSN. The CB has a very high blood flow for its size and receives blood from the common carotid artery, namely the CB artery (Gonzalez *et al*, 1994). Blood is

drained from the organ via a venous plexus into the internal or external jugular veins (Kumar & Prabhakar, 2012).

Figure 1.

A schematic showing the anatomy of the carotid body. A.) The carotid body sits at the bifurcation of the common carotid artery (CC) into the external carotid artery (EC) and the internal carotid artery (IC). The carotid sinus nerve receives afferents from type I cells in the carotid body. B.) The carotid bodies contain the excitable type I cells which form synapses with afferent carotid sinus nerves as well as glia-like type II cells.

Figure 1.

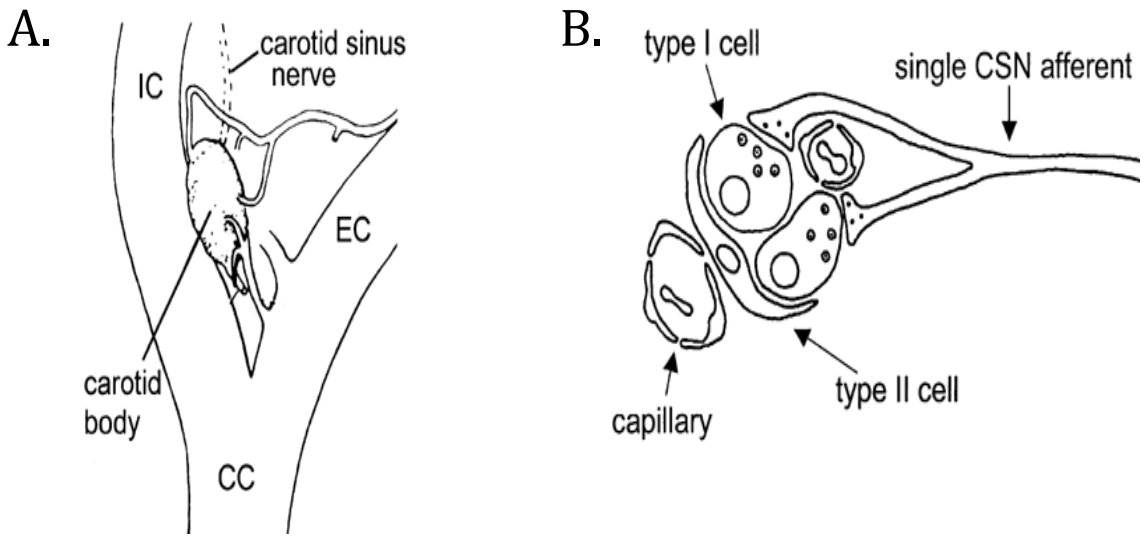
A.
carotid sinus nerve
IC
EC
carotid body
CC
B.
type I cell
single CSN afferent
type II cell
capillary

The Carotid Body and the Control of Breathing

The CB has dual innervation. First, the afferent innervation for the CB is the CSN, a branch of cranial nerve IX, the glossopharyngeal nerve, whose cell bodies lie in the petrosal ganglion (Kumar & Prabhakar, 2012). The CSN communicates with type I cells of the CB and projects to the nucleus tractus solitarius (NTS) of the medulla (Finley and Katz, 1992). The second innervation to the CB is the ganglioglomular nerve carrying efferent sympathetic fibers from the superior cervical ganglion to the organ (Gerard & Billingsly, 1932). The ganglioglomular nerve innervates blood vessels in the CB to control blood flow to the organ (Gonzalez *et al*, 1994).

When blood is perfused through the organ, it is monitored by the chemosensitive type I cells. In response to stimuli, such as hypoxia, type I cells elicit an acute hypoxic response (Figure 2). First, K^+ channels on the plasma membrane are inhibited (Lopez-Barneo *et al*, 1988) which results in a membrane depolarization. While the mechanism behind this inhibition is still debated, the K^+ channels that play a major role in the hypoxic response in rats are the TASK-like "leak" channels and the BK_{Ca} channels (Buckler, 1997; Peers, 1990; Lopez-Barneo, 2004). The membrane depolarization then causes voltage-gated Ca^{2+} channels (mainly L and P/Q type) to open, resulting in an increase of intracellular calcium ($[Ca^{2+}]_i$) (Buckler & Vaughan-Jones, 1994). An increase in $[Ca^{2+}]_i$ results in neurotransmitter release from type I cells and an increased firing rate of the CSN to the NTS of the medulla. From there, the NTS integrates information and interacts with the ventral breathing centers of the pons and medulla to produce an efferent

Figure 2.

A schematic showing the acute hypoxic response in a type I carotid body cell. Adverse stimuli sensed by type I cells cause the following cascade of events: K^+ channels are inhibited causing a membrane depolarization. This depolarization opens voltage-gated calcium channels, increasing the amount of intracellular calcium ($[Ca^{2+}]_i$). A rise in $[Ca^{2+}]_i$ causes more neurotransmitters (NT vesicles) to be released onto the carotid sinus nerve (CSN), increasing the firing rate to the nucleus tractus solitarius (NTS), ultimately resulting in hyperventilation.

Figure 2.

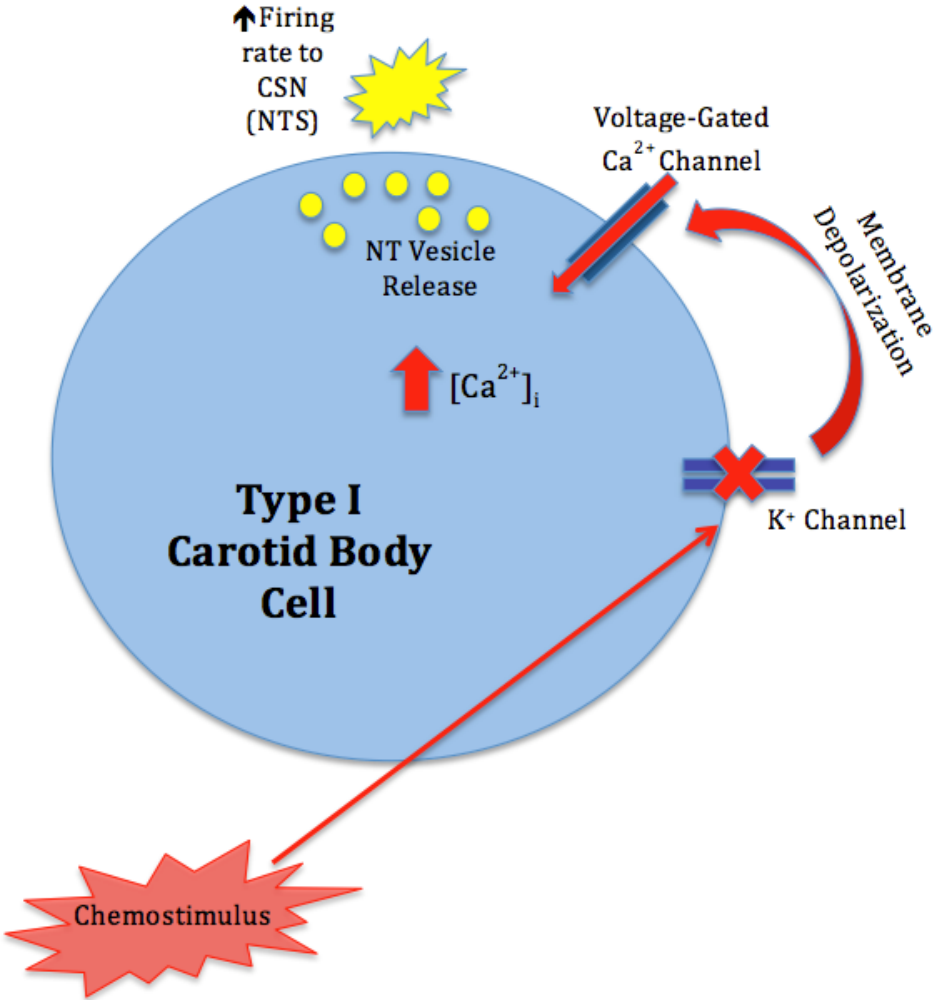
↑Firing rate to CSN (NTS)
Voltage-Gated Ca^{2+} Channel
NT Vesicle Release
Membrane Depolarization
$[Ca^{2+}]_i$
Type I Carotid Body Cell
K^+ Channel
Chemostimulus

response through the phrenic nerve and other ventilatory and cardiovascular reflexes. These reflexes ultimately increase O_2 levels in the blood back to homeostatic levels (Teppema & Dahan, 2010; Gonzalez *et al*, 1995).

Neurotransmitters Released by Type I Carotid Body Cells

The rise in $[Ca^{2+}]_i$ causes the release of many neurotransmitters into the synaptic cleft between the type I cell and the CSN. The neurotransmitters can then act presynaptically (in a paracrine or an autocrine fashion) onto type I cells or postsynaptically on the CSN. The interplay between inhibitory and excitatory neurotransmitters determines the CB's effect on the CSN.

Acetylcholine & ATP

Acetylcholine (ACh) was identified as the first possible transmitter in the CB (Schweitzer & Wright, 1938). Along with ACh, the enzymes to synthesize and degrade ACh, choline acetyltransferase and acetylcholinesterase, respectively, are also found in the rat CB type I cells (Nurse, 1987). Once released from a type I cell, ACh can activate two different cholinergic receptors: nicotinic and muscarinic ACh receptors, which are both found presynaptically on type I cells and postsynaptically on the CSN (Wyatt & Peers, 1993; Shirahata *et al*, 2007). ACh is inhibitory via the muscarinic receptors and excitatory via the nicotinic receptors.

The role of ACh in chemotransduction has been debated due to the findings that when cholinergic receptors are blocked, the afferent nerves still depolarize during a hypoxic stimulus (Zhang *et al*, 2000). It was discovered that a second

neurotransmitter, adenosine triphosphate (ATP), is co-released from type I cells with ACh (Zhang *et al*, 2000). ATP binds to P2X receptors located on the CSN and together, ACh and ATP are the main excitatory neurotransmitters released from type I cells (Zhang *et al*, 2000). It is important to note that ATP can act inhibitory because it also binds to P2Y receptors on type I and type II cells, which may act as a protective negative feedback mechanism (Xu *et al*, 2003; Xu *et al*, 2005).

Dopamine

Dopamine (DA) is the main catecholamine found in the dense core vesicles of type I cells of rats (Vicario *et al*, 2000). DA is made by an enzyme typical of type I cells, tyrosine hydroxylase (TH), which converts tyrosine to DA. DA binds to D_2 receptors present on both the CB and the CSN (Lazarov *et al*, 2009; Dinger *et al*, 1981; Mir *et al*, 1984). DA is typically an inhibitory monoamine in most mammals (Docherty & McQueen, 1978), but has been found to have excitatory effects in the rabbit CB (Gonzalez *et al*, 1994). More recently, DA has been thought of more as a neuromodulator. Under short-term (Wakai *et al*, 2010) and chronic (Wang & Bisgard, 2002) hypoxia, TH levels increase. The increased DA produced and ultimately released may act presynaptically to prevent intense hyperventilation.

Enkephalins

Opioid peptides are classified into three categories: endorphins, dynorphins, and enkephalins. Met- and leu-enkephalin are predominately found as their precursor, proenkephalin A, in the CB (Gonzalez *et al*, 1994; Gonzalez-Guerrero *et al*,

1993a,b). Leu-enkephalin (LET) expresses an inhibitory effect on the pre-Bötzinger complex and the ventrolateral part of the NTS resulting in decreased respiratory rate (Inyushkin, 2007). Further, Gonzalez-Guerrero *et al* showed that at the level of the CB, the opioid peptides leu- and met-enkephalin are co-released with DA from type I cells (1993a,b). The co-release of DA and opioid peptides from the same dense-core vesicles could explain the dramatic decrease in respiration due to the inhibitory signal from type I cells to the postsynaptic CSN, as well as the protective feedback mechanism on the presynaptic type I cell itself.

CLASSIFICATION OF OPIOID RECEPTORS

The discovery of opioid receptors was unique because the receptor was identified before the endogenous ligand was known (Pasternak, 2013). Martin was the first to suggest the presence of multiple types of receptors, and proposed morphine receptors, which are now known as the mu (μ) opioid receptors, and nalorphine receptors, now classified as kappa (κ) opioid receptors (Martin, 1967). A decade later, Kosterlitz classified the delta (δ) opioid receptor through the use of their endogenous ligand enkephalins (Lord *et al*, 1977). Other types of opioid receptors, such as the sigma opioid receptor and the opioid receptor like-1, have been categorized, but little is known about their functions or whether they are true opioid receptors (Al-Hasani & Bruchas, 2011). For this thesis, only the well-understood μ, δ, κ opioid receptors will be examined.

Mu Opioid Receptors

The μ opioid receptors are the most studied opioid receptor due to their role in analgesia with their highly selective agonist morphine (Pradhan *et al*, 2012). Along with pain suppression, μ opioid receptor agonists can cause desired effects such as euphoria, anti-diarrhea, cough suppression, and undesirable effects like respiratory depression, constipation, vomiting, and dependence (Kelly, 2013).

The μ opioid receptors differ from the κ and δ opioid receptors in terms of exons. All three opioid receptors have seven transmembrane domains that include the first exon encoding the N-terminus and the first transmembrane domain in addition to a second and third exon, which each encode an additional three transmembrane domains. However, the μ opioid receptors have a fourth exon encoding 12 amino acids at the end of the C-terminus (Pasternak, 2013).

Kappa Opioid Receptors

κ opioid receptor activation is involved in gut motility, feeding, mood, and diuresis (Pradhan *et al,* 2012). In contrast to the other two types of opioid receptors, the antagonists specific for κ opioid receptor, like norbinaltorphimine, have effects that last up to several weeks, in contrast to naloxone, an antagonist for all three types of receptors, which only has effects for a few hours (Pradhan *et al,* 2012).

Delta Opioid Receptors

The δ opioid receptors have been linked to neuroprotection and cardioprotection when activated by their selective agonists (Feng *et al*, 2012).

Interestingly, stimulation of δ opioid receptors by JNJ-20788560 did not result in the adverse effects associated with the other opioid receptors, such as respiratory depression, constipation, and dependence (Codd *et al*, 2009). The endogenous ligands for the δ opioid receptors are enkephalins, which have been found in the CB of rabbits (Gonzalez *et al*, 1993b) and have been noted to depress chemosensory discharge from the CSN (Kirby & McQueen, 1986).

Opioid Receptors: G_i Protein Linked

All three families of opioid receptors are seven transmembrane G protein-coupled receptors that activate inhibitory G proteins (G_i) (Al-Hasani & Bruchas, 2011). Upon activation by a selective agonist, the $G_{\alpha i}$ and $G_{\beta\gamma}$ subunits dissociate and act on various intracellular pathways. Most notably, opioid receptor activation has the ability to modulate ion channels.

After opioid receptor activation and G protein dissociation (Figure 3), the $G_{\beta\gamma}$ subunit binds to voltage-gated Ca^{2+} channels (VGCC) and inhibits calcium influx decreasing the amount of $[Ca^{2+}]_i$. (Al-Hasani & Bruchas, 2011). This decreased amount of $[Ca^{2+}]_i$ then has the ability to affect downstream Ca^{2+}—dependent cellular pathways, such as neurotransmitter release.

Activation of opioid receptors also alters K^+ channel conductance as a means to reduce cellular excitability and inhibit neurotransmitter release. As the $G_{\alpha i}$ subunit dissociates and binds to K^+ channels, the increase in K^+ conductance causes the cell to hyperpolarize ultimately inhibiting downstream neurotransmitter release (Satoh & Minami, 1995; Al-Hasani & Bruchas, 2011).

Additionally, the $G_{\beta\gamma}$ subunit directly interacts with the members of the SNARE complex downstream of VGCCs through an independent mechanism (Figure 4). The $G_{\beta\gamma}$ subunit has been shown to specifically affect SNAP25 and syntaxin1A which can ultimately decrease the amount of neurotransmitter released from the type I cell. (Wells *et al*, 2012; Blackmer *et al*, 2005).

The $G_{\alpha i}$ and the $G_{\beta\gamma}$ subunits that alter the Ca^{2+} and K^{+} channel conductance are sensitive to pertussis toxin (PTX). PTX catalyzes the ADP-ribosylation of G proteins and by doing so prevents the agonist-induced dissociation of the proteins into active subunits (Katada *et al*, 1984; Holz *et al*, 1986).

Figure 3.

A schematic showing the effect of opioid receptor activation on VCGGs. Upon activation by their selective agonists, all three families of opioid receptors (μ, κ, δ) respond by activating G_i proteins. The $G_{\beta\gamma}$ subunit binds directly to VGCCs and inhibits Ca^{2+} influx resulting in a decrease of $[Ca^{2+}]_i$.

Figure 3.

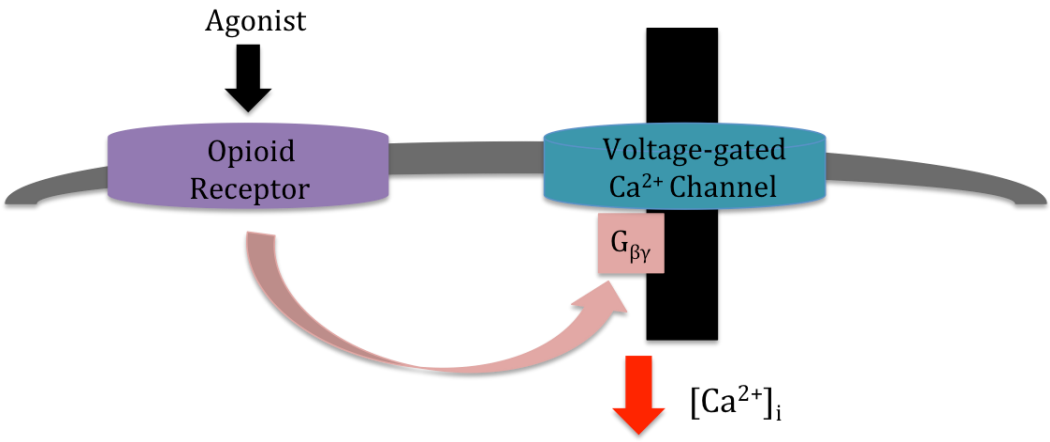
Agonist
Opioid Receptor
Voltage-gated Ca^{2+} Channel
$G_{\beta\gamma}$
$[Ca^{2+}]_i$

Figure 4.

A schematic showing the activation of an opioid $G_{\beta\gamma}$ subunit binding directly to both VGCCs and the neurotransmitter (NT) synaptic machinery (i.e. SNARES and SNAP proteins) involved in secretory granule exocytosis.

Figure 4.

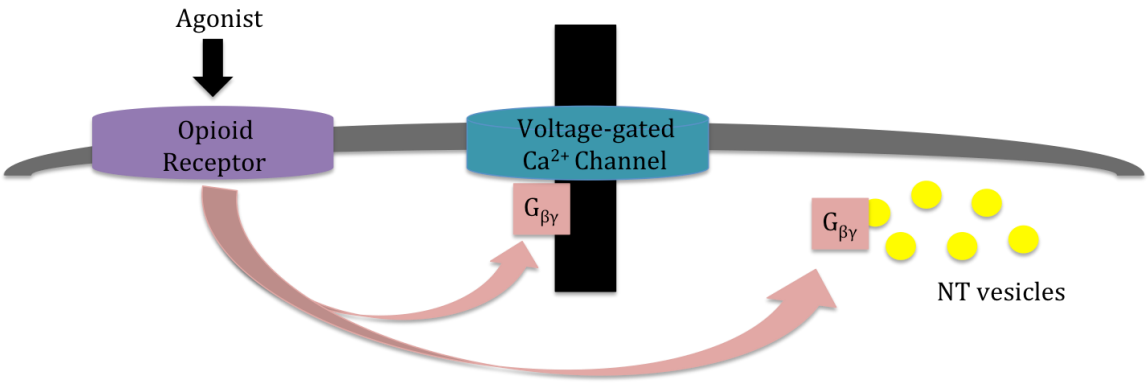
Agonist
Opioid Receptor
Voltage-gated Ca2+ Channel
Gβγ
Gβγ
NT vesicles

OPIATES AND BREATHING

The drive to breath is generated in the brainstem and is modulated by inputs from the cortex, central chemoreceptors located in the brainstem, and peripheral chemoreceptors, such as the CB and the aortic bodies. The main respiratory centers include the pre-Bötzinger complex, the retro-trapezoid and parafacial respiratory group, the locus coeruleus in the pons, and the NTS (Pattinson, 2008; Greer *et al*, 1995; Han *et al*, 1997).

It has been shown that there is a high concentration of opioid receptors in areas of the brain related to respiration (Mutolo *et al*, 2007; Mansour & Watson, 1993). Activation of opioid receptors in these respiratory centers of the brain and brainstem affects ion channels through G_i proteins, which can alter the excitability of neurons and ultimately affect respiration patterns. At low doses, opioids change the respiratory patterns whereas at high doses, they reduce tidal volume (Lalley, 2003).

Ballanyi *et al* proposed after a study in newborn mouse brainstem slices that the depression of breathing by opioids is caused by the postsynaptic K^+ channel hyperpolarization of inspiratory neurons in the pre-Bötzinger complex (2010). On a bigger scale, opioids blunt respiratory responsiveness to CO_2 and hypoxia, depress the rate and depth of breathing, increase upper airway resistance and reduce pulmonary compliance (Feng *et al*, 2012).

Specifically, μ opioid receptor activation decreases respiratory rate and can lead to complete apnea upon overdose (Feng *et al*, 2012). The μ opioid receptor agonist, DAMGO caused a naloxone-reversible, dose-dependent decrease in the

frequency of respiratory rhythmic discharge when applied to the bathing solutions of the neonatal rat brainstem (Greer *et al*, 1995). Furthermore, the activation of μ opioid receptors in the NTS eliminated the hypoxic ventilatory response in rats (Zhang *et al*, 2011). Overall, these studies show that opioids can affect the acute hypoxic response and ultimately the respiration patterns in rodents via the central nervous system.

The primary efferent nerve involved in respiration is the phrenic nerve. The phrenic nerve innervates the diaphragm muscle, the main muscle of inspiration. It has been shown that U50-488, a selective agonist for the κ opioid receptor, causes a dose-dependent reduction in phrenic nerve discharge when studied in decerebrated cats (Haji & Takeda, 2001).

Activation of δ opioid receptors has a less pronounced effect on breathing. *In vitro*, the addition of [D-Pen2,5]enkephalin, a δ opioid receptor agonist, did not affect the respiratory burst frequency or the amplitude (Greer *et al*, 1995). However, it is important to note that no opioids lack respiratory side effects (Pattinson, 2008).

Alternatively, in the peripheral nervous system, no opioid signaling research has been done on isolated type I CB cells; only whole CBs have been examined. In studies in which fentanyl was used with canine carotid bodies, it was found that carotid chemoreception increases the respiratory drive while fentanyl, a common opioid, decreases the respiratory drive (Mayer *et al,* 1989). It has been shown that activation of opioid receptors in the peripheral nervous system inhibits the acute hypoxic response, but the mechanism is still not known (Kirby & McQueen, 1986).

HYPOTHESIS

It has been demonstrated that activation of opioid receptors in the CBs can inhibit the acute hypoxic response (Kirby & McQueen, 1986); however, the mechanism behind this inhibition is not yet understood. Activation of opioid receptors alters the mechanisms by which neurotransmitters are released by affecting ion channels directly. This thesis will test the hypothesis that activation of opioid receptors on the type I cells of the rat CB may inhibit the influx of Ca^{2+} via G_i-protein coupled receptors, reducing neurotransmitter release, decreasing the firing rate of the CSN and ultimately inhibiting the acute hypoxic response.

SUMMARY

The CBs are the primary peripheral chemoreceptors located at the bifurcation of the common carotid arteries. In response to adverse changes in blood gases, such as an increase in CO_2 or a decrease in O_2, the chemosensitive type I cells depolarize and release neurotransmitters onto the CSN. The CSN then relays the information via the glossopharyngeal nerve to the NTS in the brainstem, which ultimately causes hyperventilation to restore homeostasis.

To test the hypothesis of this thesis, immunofluorescence can identify which opioid receptors are present on rat carotid body type I cells. Next, calcium imaging can examine the effects of receptor activation by their selective agonists. Finally, calcium imaging can also help characterize the effects seen to identify the mechanism by which opioids inhibit the CB-driven acute hypoxic response in the peripheral nervous system.

MATERIALS AND METHODS

All studies described in this paper were performed in accordance with protocols approved by the Wright State University Institutional Laboratory Animal Care and Use Committee (IACUC). These protocols are in accordance with the National Institute of Health guide for the care and use of laboratory animals (NIH publications No. 80-23) revised 1996.

DISSECTION AND DISSOCIATION OF NEONATAL RAT CAROTID BODY TYPE I CELLS

On experimental days, three or four neonatal Sprague Dawley rats (aged 10-20 days) were placed in an induction chamber supplied with 4.5% isofluorane and oxygen to initially anesthetize the animal. When the animal reached unconsciousness, it was transferred from the induction chamber to a nose cone supplying the same anesthetic gas. To ensure that the animal was completely anesthetized, the foot pinch withdrawal reflex was tested. Only after no reflex was seen were the following experimental procedures taken: The rat's forelegs were taped down to reduce any movement and an incision was made along the rat's sternum to expose underlying subcutaneous fascia. This fascia, the salivary glands, and the skeletal muscles lateral to the trachea were removed using very fine forceps (Moria, Fine Science Tools, USA), which exposed the common carotid artery while being careful not to cut or damage any adjacent blood vessels.

The remainder of the dissection was done under a low magnification microscope (Omâno, Japan). Once the common carotid artery became visible, any remaining fat and fascia was removed to observe the bifurcation of the common

carotid into the internal and external carotid arteries. After removal of the glossopharyngeal nerve and the reflection of the occipital artery, the carotid body, usually adhered to the internal carotid artery by connective tissue, became visible in the bifurcation. The organ was then carefully pinched off using forceps and placed directly into ice cold, oxygenated, Dulbecco's phosphate buffered saline (DPBS) without Ca^{2+} or Mg^{2+} (Sigma). Following the extraction of the carotid body, the rats were euthanized via decapitation while still deeply anesthetized and disposed of in accordance with Lab Animal Research specifications. The six to eight carotid bodies were then returned to the lab and cleaned of any remaining connective tissue under the dissection Omâno microscope.

The cleaned carotid bodies were then transferred to a digestive enzyme solution (0.4 mg/ml collagenase type I, 249 u/mg (Worthington Biochemical Corporation), 0.2 mg/ml trypsin type I, 10,000 BAEE u mg^{-1} (Sigma) in DPBS with low $CaCl_2$ (86 μM) and $MgCl_2$ (350 μM)) and incubated for 20 minutes at 37˚C to dissolve the connective tissue holding the carotid body together. Then, the carotid bodies were teased apart and incubated for another 7 minutes at 37˚C. The tissue was removed from the Petri dish and transferred to a test tube using a fire polished, silanized (Sigmacote, Sigma) Pasteur pipette where it was centrifuged at 110g for 5 minutes. The cells were resuspended in tissue culture medium, (Ham's F12 (Sigma) supplemented with 10% heat inactivated fetal bovine serum (Biowest)) triturated, and centrifuged for another 5 minutes at 110g. Finally, the cells were resuspended in tissue culture medium and plated onto 22mm^2 poly-D-lysine (Sigma) coated coverslips (Fisher Scientific) for immunofluorescence or 15mm diameter

poly-D-lysine coated coverslips (Warner Instruments) for Ca^{2+} imaging. Coverslips were placed in 35mm Petri dishes and maintained at 37˚C in a humidified, 5% CO_2/air incubator for 2 hours to allow the cells to adhere to the coverslips.

IMMUNOFLUORESCENCE

Coverslips with adhered type I cells were fixed by immersion in methanol at -20˚C for 15 minutes. Cells were then washed 3 x 5 minutes with a permeabilization and blocking solution (0.3% triton X-100 and 1% bovine serum albumin in phosphate buffered saline (PBS)) which allowed antibodies to enter the cell and limited unspecific binding of the anti-opioid receptor antibodies to reduce background or nonspecific staining. Specific primary antibodies were used to identify the different three opioid receptors while an anti-TH antibody identified the cells as type I cells.

The anti-δ opioid and the anti-μ opioid receptor 1˚ antibodies (Santa Cruz Biotechnology: sc-9111, sc-15310) were rabbit polyclonal antibodies diluted to 1:200 with the blocking solution, whereas the anti-κ opioid receptor 1˚ antibody (USBiological, O7030-31A) was a rabbit polyclonal antibody diluted to 1:1000 with the blocking solution. All primary antibodies were added to the appropriate coverslips with the anti-TH 1˚ antibody (Sigma) at a dilution of 1:1000 in blocking solution and incubated at 4˚C for 16 hours.

Following the incubation with the 1˚ antibodies, coverslips were washed 2 x 10 minutes with the blocking solution and then incubated for 2 hours in the dark at room temperature with the 2˚ antibodies diluted to 1:200 with the blocking

solution. In the first set of experiments, the antibodies used were a Rhodamine Red-X-conjugated AffiniPure donkey anti-sheep IgG 2˚ antibody which identified the TH and a Fluorescein (FITC)-conjugated AffiniPure donkey anti-rabbit IgG 2˚ antibody which marked the specific opioid receptors (Figure 5). Due to poor control experiments (Figure 9) in which no 1˚ antibodies were added to the coverslips and the 2˚ antibody for TH was non-specifically binding, a second set of experiments were conducted with a Rhodamine Red-X-conjugated AffiniPure donkey anti-rabbit IgG 2˚ antibody marking the opioid receptors and a Fluorescein (FITC)-conjugated donkey anti-mouse IgG 2˚ antibody identification of TH (Figure 6). All 2˚ antibodies were supplied by Jackson Immunoresearch. The δ opioid receptors have previously been shown to be present in dorsal root ganglion cells (Zhang & Bao, 2012); therefore, a positive control experiment was used to test the validity of the anti-δ opioid receptor 1˚ antibodies (Figure 7).

Immunofluorescence images were acquired using a DeltaVision microscope system (Applied Precision) on an inverted Olympus IX71 microscope with an oil immersion, x63 magnification, 1.4 n.a. objective and Coolsnap HQ CCD camera (Photometrics). Images were acquired with settings for a 768 x768 image size, RD•TR•PE 617/73 nm emission and 555/28 nm excitation, FITC 528/38 nm emission and 490/20 nm excitation, and a DAPI 457/50 nm emission and 360/40 nm excitation. Multiple Z-sections were taken through each cell and the images were deconvolved through the Softworx software to reassigned out-of-focus light (Applied Precision).

Figure 5. Opioid receptor staining in isolated carotid body type I cells using double immunofluorescence. In the first set of experiments, the 1˚ antibody identified the receptors while the 2˚ antibodies, which are fluorescent, stained tyrosine hydroxylase (TH) **red** and the opioid receptors (OR) **green**. The antibodies responsible for identifying and staining the receptors are listed.

Figure 5.

Antibody	Target	Fluorochrome	Color
1˚ rabbit anti-rat	μ, δ, κ opioid receptors	Fluorescein (FITC)	Green
2˚ donkey anti-rabbit			
1˚ sheep anti-rat	Tyrosine Hydroxylase	Rhodamine	Red
2˚ donkey anti-sheep			

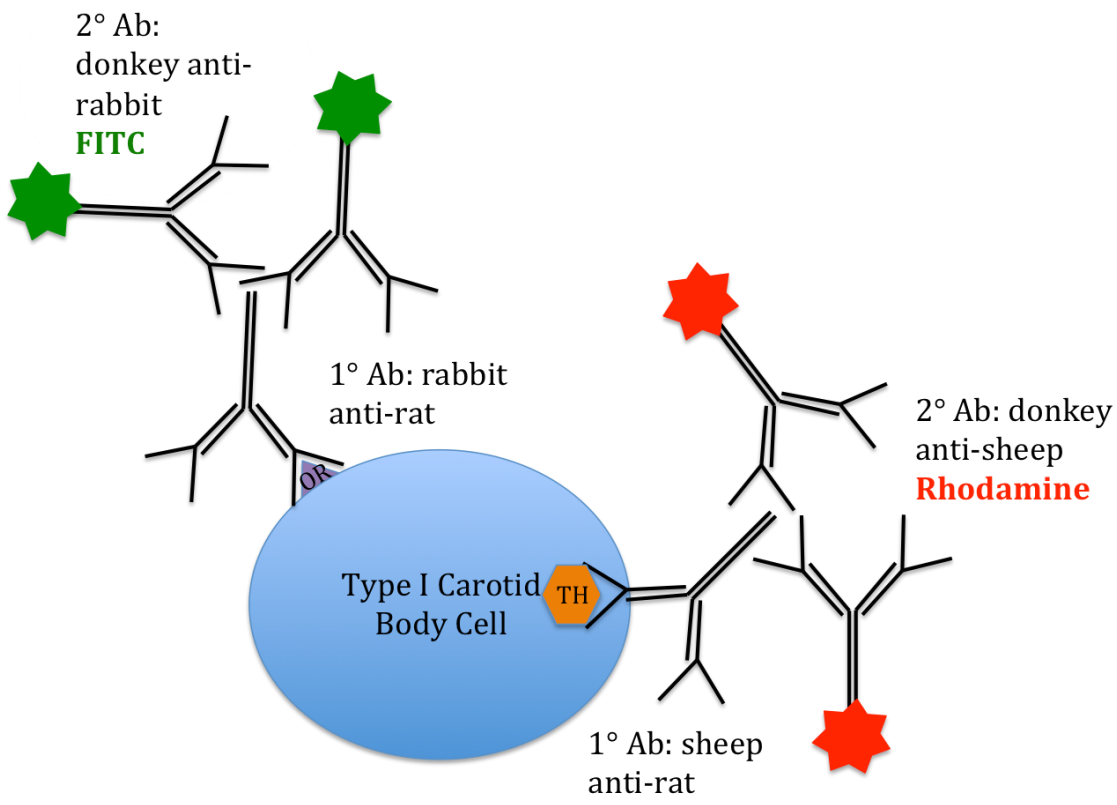

Figure 6. Opioid receptor staining in isolated carotid body type I cells using double immunofluorescence. In the second set of experiments, the same 1˚ antibodies identified the receptors, but the new 2˚ antibodies stained the tyrosine hydroxylase (TH) **green** and the opioid receptors (OR) **red**. The 1˚ and 2˚ antibodies responsible are listed.

Figure 6.

Antibody	Target	Fluorochrome	Color
1˚ rabbit anti-rat	μ, δ, κ opioid receptors	Rhodamine	Red
2˚ donkey anti-rabbit			
1˚ mouse anti-rat	Tyrosine Hydroxylase	Fluorescein (FITC)	Green
2˚ donkey anti-mouse			

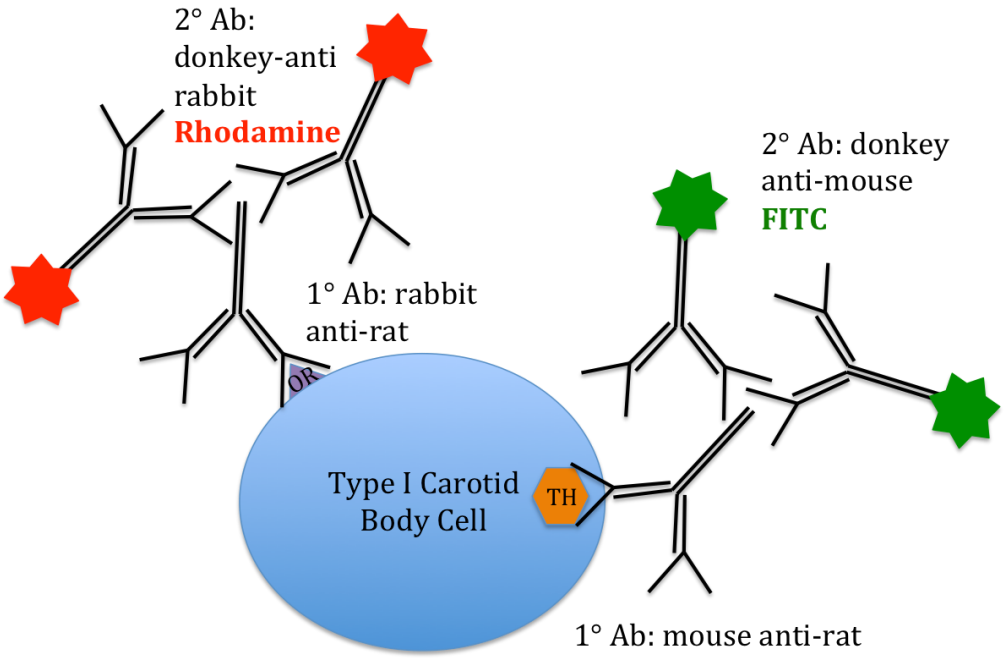

Figure 7. Delta opioid receptor staining in dorsal root ganglion (DRG) cells. The 1˚ and 2˚ antibodies used to identify and stain the δ opioid receptors (OR) **green** are listed.

Figure 7.

Antibody	Target	Fluorochrome	Color
1˚ rabbit anti-rat	δ opioid receptors	Fluorescein (FITC)	Green
2˚ donkey anti-rabbit			

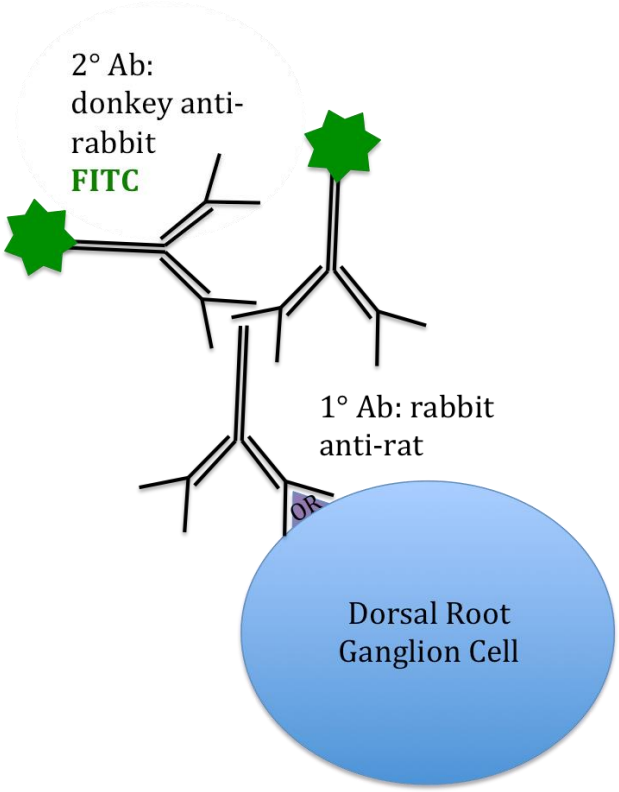

FURA-2AM

Fura-2AM is a molecular probe used to determine intracellular calcium concentrations through fluorescence (Figure 8). The acetoxymethyl ester portion of the probe allows the molecule to diffuse through the plasma membrane of the cell, which avoids using more invasive techniques for loading. Once the probe is inside the cell, the cell's esterases cleave off the acetoxymethyl portion, leaving the cell-impermeant fluorescent indicator behind. Upon binding Ca^{2+}, Fura-2 exhibits an absorption shift that can be observed by scanning the excitation spectrum between 300 and 400 nm, while monitoring the emission at ~510 nm (invitrogen.com). In these imaging experiments, the Fura-2 was excited by exposure to both 340 nm and 380 nm wavelengths of light while monitoring emissions at 510 nm. Calculations made by looking at the ratios of emitted light evoked by 340 nm/380 nm excitation allowed us to determine the intracellular concentration of calcium at specific moments in time due to this formula:

$$\mathbf{[Ca^{2+}] = Kd\ (S_{f2}/S_{b2})(R_{exp}\text{-}R_{min}/R_{max}\text{-}R_{exp})}$$

$Kd = 224 \times 10^{-9}$ M
S_{f2} = intensity 380 nm Ca^{2+} free
S_{b2} = intensity 380 nm Ca^{2+} saturated
R_{exp} = measured experimental ratio
R_{max} = Ca^{2+} saturated ratio
R_{min} = 0 Ca^{2+} ratio

Thus, the measured experimental ratio is directly proportional to the calcium concentration in the cell and can be calculated by calibrating the system using a 0 nm Ca^{2+} solution and a saturating Ca^{2+} solution which is typically 5 mM. All fluorescent values in this research are given as ratio units rather than Ca^{2+} concentrations because previous students in the Wyatt laboratory have not been able to acquire satisfactory S_{b2} readings. Furthermore, by using two different

wavelengths of light to measure concentration, variables such as dye bleaching and cell thickness can be eliminated which prevents unwanted artifact.

CALCIUM IMAGING

Cells were visualized with a Nikon Eclipse TE2000U inverted microscope with a CFI super fluor x40 oil immersion objective. Fura-2 was excited with 50 msec exposures to 340 nm and 380 nm light at 0.2 – 0.5 Hz using a Lambda 10 – 3 filter wheel (Sutter) and emitted fluorescence measured at 510 nm using a CoolSNAP HQ2 CCD camera. Light was provided by a Lambda-LS xenon arc lamp (175 watt, Sutter). Because of the high wattage of this lamp, the light first passed through neutral density filters of 0.7 optical densities (Chroma, USA) before reaching the isolated cells to prevent any cell photodamage.

Data acquisition and analysis was completed using Metafluor 7.1.2 imaging software (Molecular Devices). The 340/380 ratio images were generated online after regions of interest were placed around cells to show changes in the fluorescence ratio over time.

Figure 8. Fluorescence emission of Fura-2 at differing wavelengths. This graph shows the varying fluorescence of Fura-2 due to excitation wavelength and intracellular free-calcium concentration. The dye was excited at wavelengths listed along the x-axis. When the intracellular calcium level is zero, the fluorescence intensity at 340 nm is less than the intensity at 380 nm when viewed at 510 nm. As the free calcium level increases, the fluorescence intensity at 340 increases as the fluorescence intensity at 380 nm decreases as viewed at 510 nm. Image from Molecular Probes.

Figure 8.

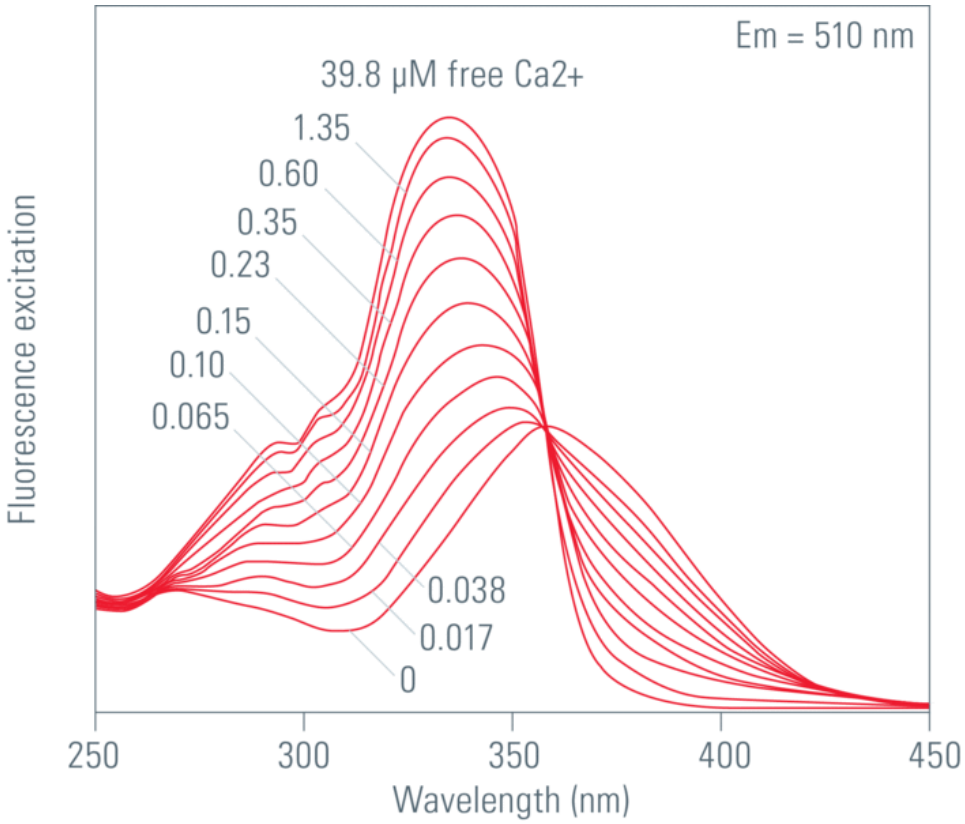
Em = 510 nm
39.8 µM free Ca2+
1.35
0.60
0.35
0.23
0.15
0.10
0.065
0.038
0.017
0
Fluorescence excitation
250
300
350
400
450
Wavelength (nm)

PERFUSION OF ISOLATED TYPE I CAROTID BODY CELLS

Isolated cells, plated on 15 mm round coverslips, were placed into the perfusion chamber and washed with HEPES buffered saline solution (NaCl 140mM, KCl 4.5mM, $CalCl_2$ 2.5mM, $MgCl_2$ 1mM, Glucose 11mM, HEPES 10mM; pH to 7.57 with NaOH) for approximately 5 minutes. Temperatures were maintained between 34°-36°, keeping the final pH 7.4, by passing solutions through an in-line heater (SH-27F, Warner Instruments, USA) which was controlled by feedback to an automatic temperature controller (TC-344B, Warner Instruments, USA).

The dissociation process yields predominately individual, isolated type I cells, with sporadic clusters of cells. Regions of interest (ROI) were drawn over cells using the Metafluor software and the calcium signal was taken within the ROI. Changes in the calcium signal were measured from the baseline to the peak response during exposure. Only cells that responded to a 80mM K^+ HEPES stimulus (NaCl 64.5mM, KCl 80mM, $CalCl_2$ 2.5mM, $MgCl_2$ 1mM, Glucose 11mM, HEPES 10mM; pH to 7.57 with KOH; 80mM KCl was used to evoke maximal Ca^{2+} influx) with a rapid increase in fluorescence ratio, recovered back to the predetermined baseline, showed no spontaneous Ca^{2+} spiking, and had steady baselines were used in this study. The complete recovery from the K^+ stimulus had to occur to ensure that the Ca^{2+} handling properties of the type I cell were healthy. Recording from individual cells represents n=1. Compounds (Table 1) were only applied to a coverslip once to avoid the possibility of desensitization or sensitization.

Solution changes occurred by switching the solution inflow to a chamber containing the solution of choice. The solutions were perfused by gravity and the exchange was usually complete within 15 seconds.

STATISTICAL SIGNIFICANCE

Data are presented as means ± standard error of the mean. Differences between individual means were determined by an unpaired student's t-test. A value of $p<0.05$ was taken to indicate statistical significance.

CHEMICALS

The drugs used in this research are included in Table 1.

Table 1.

Compound	Target	Source
[D-Ala^2, N-Me-Phe^4, Gly^5-ol]-enkephalin acetate salt (DAMGO)	μ opioid receptor	Sigma-Aldrich
U50-488 hydrochloride	κ opioid receptor	Sigma-Aldrich
Pertussis Toxin	G_i protein	Sigma-Aldrich

RESULTS

IMMUNOFLUORESCENCE

Immunofluorescence was used to identify which of the opioid receptors (μ, κ, or δ) were present on the membranes of rat CB cells type I cells. TH identified the cells as type I cells while DAPI (blue) identified the nucleus. Control experiments were only treated with the 2° antibodies; no 1° antibodies were applied to the control coverslips. Images were acquired using a DeltaVision microscope and each image represents an example z-section through the cell. Results are described qualitatively rather than quantitatively.

Type I Cells

From the images, staining can be seen for both the μ opioid receptors and the κ opioid receptors but little to no staining is seen for δ opioid receptors (Figure 9). The staining for the μ and κ opioid receptors is targeted to the cytoplasm and cell membrane whereas the majority of δ staining is found in the nucleus, which may be nonspecific. However, in this set of experiments, our control images showed nonselective red staining of the 2° antibody for TH. This is abnormal because the controls were not treated with the 1° antibodies. Because of this, a second experiment was performed with a new 1° antibody for TH and new 2° antibodies for both the opioid receptors and for TH.

In the second set of experiments, there was staining for both the μ and the κ opioid receptors, but very faint staining was seen for the δ opioid receptors (Figure 10). The brightest staining for the μ and κ opioid receptors was in the cytoplasm

and on the cell membrane. The control images were clear of any nonselective 2° antibody staining showing that our 2° antibody was more selective and only binding to our 1° antibodies when present.

Figure 9. Opioid receptor staining in isolated rat CB type I cells using double immunofluorescence. The 2˚ antibodies stained the opioid receptors **green** and tyrosine hydroxylase (TH) **red** while DAPI stained the nucleus **blue**. Staining is present for μ and κ opioid receptors and is not present for δ opioid receptors. Control image shows nonselective staining for the TH 2° antibody even when the 1° antibody was absent. All images are 15 microns.

Figure 9.

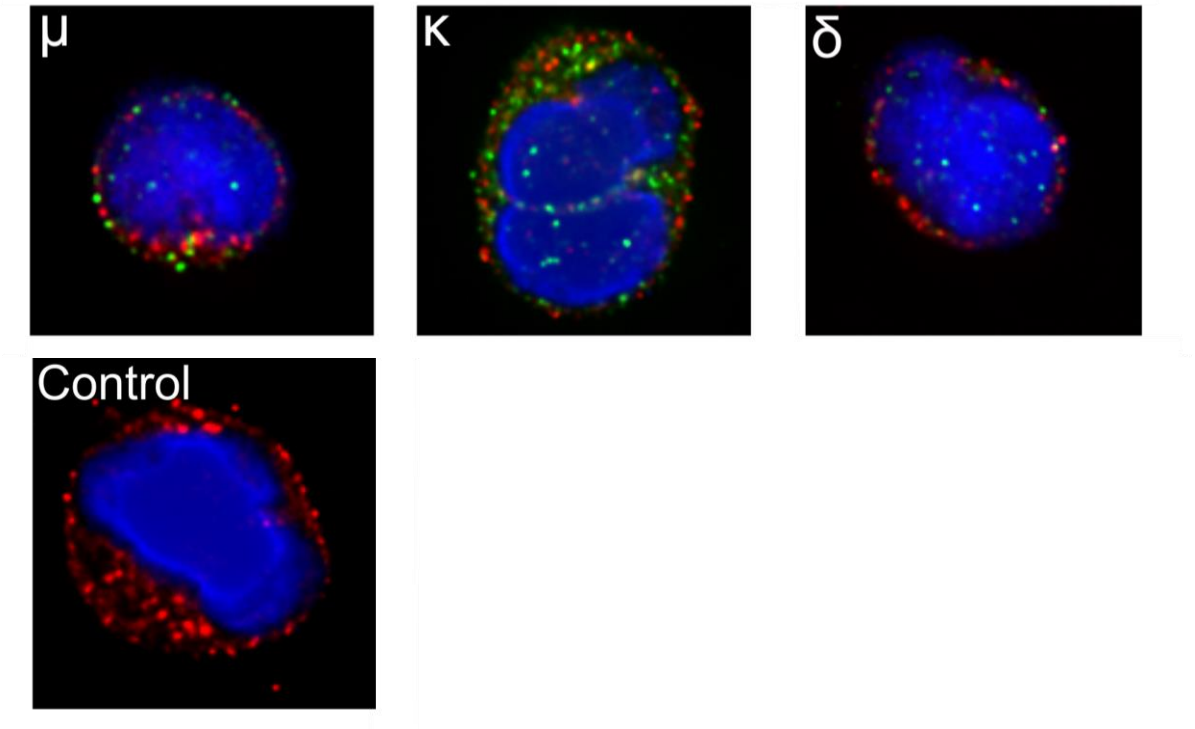

Figure 10. Opioid receptor staining in isolated rat CB type I cells using double immunofluorescence. The receptors, tyrosine hydroxylase (TH), and the nucleus are all shown in 16-bit greyscale. The 2˚ antibodies stained the opioid receptors **red** and TH **green** while DAPI stained the nucleus **blue** in the merged images. Staining is present for μ and κ opioid receptors and is not present for δ opioid receptors. TH is seen throughout the cytoplasm of μ, κ, and δ stained cells. Control images show absence of 2° antibody staining when 1° antibodies were absent. Images for the controls, μ, and κ are scaled to 15 microns. Images for δ staining are scaled to 20 microns.

Figure 10.

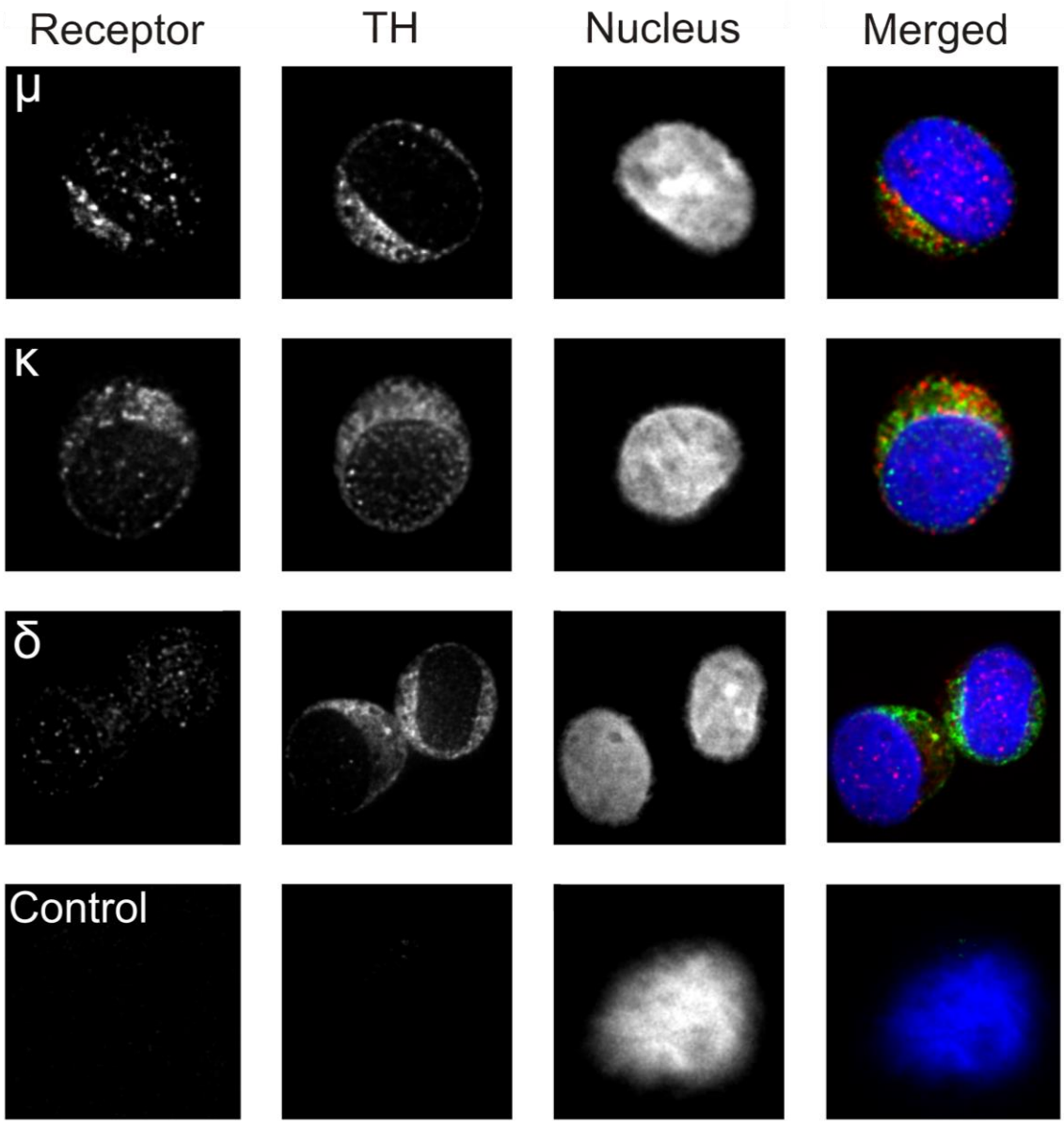

Dorsal Root Ganglion Cells

To test the integrity of the 1° antibody for the δ opioid receptor, a positive control experiment was performed on rat dorsal root ganglion (DRG) cells. DRG cells were chosen because δ opioid receptors have previously been shown in this cell type (Zhang & Bao, 2012). From these images (Figure 11), it can be concluded that our δ 1° antibody worked to identify the δ opioid receptor in the previous experiment. The δ opioid receptor has minimal staining in the nucleus, but can be seen with very pronounced staining in the cell membrane and cytoplasm of the DRG cell. The control DRG cell was not treated with 1° antibodies and is clear of any nonselective 2° antibody staining.

From these immunohistochemistry experiments, it can be concluded that μ and κ opioid receptors are present on rat CB type I cells whereas δ opioid receptors are not present. This is the first classification of opioid receptors on rat CB type I cells.

CALCIUM IMAGING

A concentration of 80mM K^+ was applied to the cells to ensure that they were viable. Only cells that responded to the stimulus with a rapid and reversible rise in $[Ca^{2+}]_i$ were chosen. Cells were then exposed to the agonist (DAMGO for the μ opioid receptor; U50-488 for the κ opioid receptor) for a minimum of 4 minutes before a 80mM K^+ stimulus was applied in the presence of the agonist. Finally, a third 80mM K^+ stimulus was applied to the cell to ensure that the cell was still viable. The control cells did not have an agonist applied.

Figure 11. Opioid receptor staining in rat DRG cells. The 2˚ antibody stained the opioid receptors **green** while DAPI stained the nucleus **blue**. The δ opioid receptors are targeted to the cytoplasm and cell membrane. Bright, punctate δ opioid receptor staining showed that the 1˚ antibody is binding to the receptors which then can confirm that δ opioid receptors are absent from type I rat CB cells. Images are scaled to 15 microns.

Figure 11.

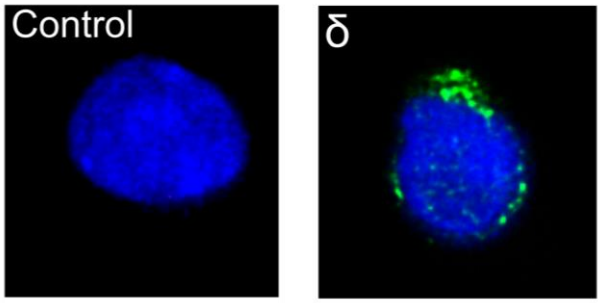

Controls

Isolated rat CB type I cells experienced a reduction in voltage-gated Ca^{2+} influx upon repetitive stimulation by the 80mM K^+ stimulus. Among 12 cells, there was an average reduction of 12.99 ± 1.46% between the first and second K^+ responses. Therefore, to analyze the effect of an agonist, the percent reduction in the controls was compared to the percent inhibition in the presence of the agonist, using an unpaired student's t-test (Figure 12).

Effect of 1μM DAMGO

DAMGO was chosen as the μ opioid receptor agonist because of proven selectivity in isolated neuronal cells (Greer *et al*, 1995; Kelly, 2013; Handa *et al*, 1981). In the presence of 1μM DAMGO (N=7), there was an average inhibition of voltage-gated Ca^{2+} influx of 9.59 ± 2.77% between the first and second K^+ responses, with the second response in the presence of DAMGO (Figure 13). Compared to the controls, 1μM DAMGO does not have a statistically significant ($p<0.25$) effect on the voltage-gated Ca^{2+} influx.

Effect of 1μM U50-488

U50-488 was chosen as the κ opioid receptor agonist because of its selectivity toward the κ opioid receptor and its poor affinity for the μ opioid receptor (Clark & Pasternak, 1988; Dayanithini *et al*, 1992). In the presence of 1μM U50-488 (N=7), there was an average inhibition of voltage-gated Ca^{2+} influx of 14.04 ± 1.89% between the first and second K^+ responses, with the second response in the

presence of U50-488 (Figure 13). Compared to the controls, 1μM U50-488 does not have a statistically significant ($p<0.67$) effect on the voltage-gated Ca^{2+} influx.

Figure 12. Analyzing Ca^{2+} imaging results. A.) The reduction in the controls between the first two K^+ responses as indicated by the black arrow. B.) Representation of the inhibition that occurred (black arrow) between the first K^+ response and the second K^+ spike in the presence of the agonist, as noted by the blue box. To analyze the results, the average reduction seen in the controls (A) was compared to the average inhibition seen in the presence of the agonist (B) using an unpaired students t-test with a $p<0.05$.

Figure 12.

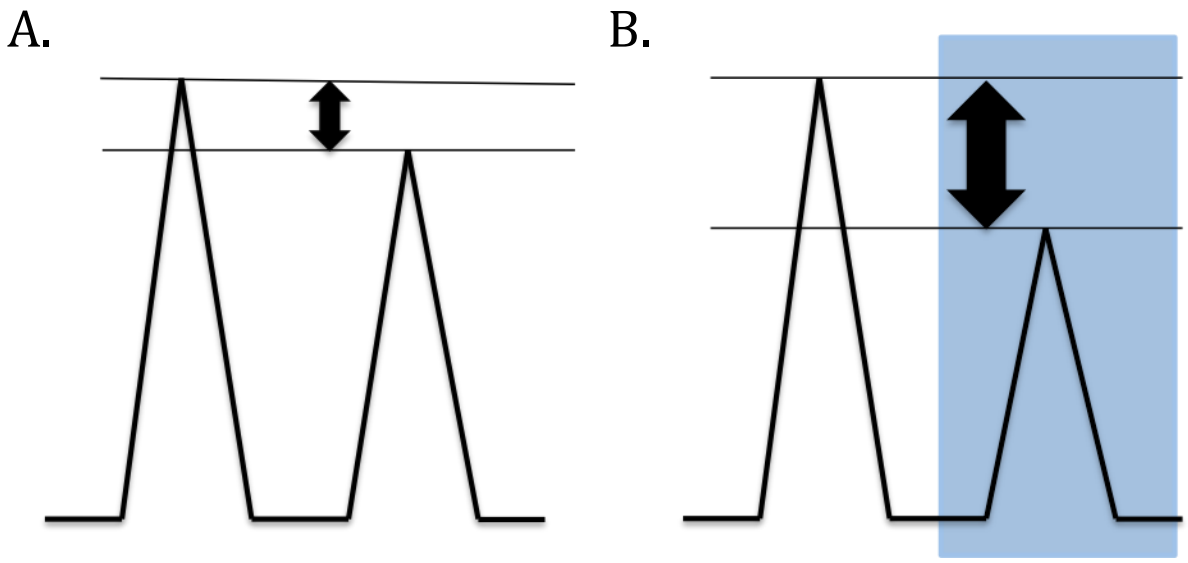

Figure 13. Effects of 1μM DAMGO and 1μM U50-488 on isolated type I CB cell Fura-2 Fluorescence ratios. The control example cell (A) shows the slight decrease in 80mM K^+-evoked Ca^{2+} entry after repeated applications of K^+ over time (N=12). Neither the example cell exposed to 1μM DAMGO (N=7), as seen by the red box (B), nor the example cell exposed to 1μM U50-488 (N=7), as seen by the green box (C), show a significant inhibition of 80mM K^+-evoked Ca^{2+} entry into the cell. The histogram (D) shows the average percent inhibitions for the controls (12.99± 1.34%), 1μM DAMGO (9.59± 2.76%) and 1μM U50-488 (14.04 ± 1.88%). Scale bar indicates 2 minutes.

Figure 13.

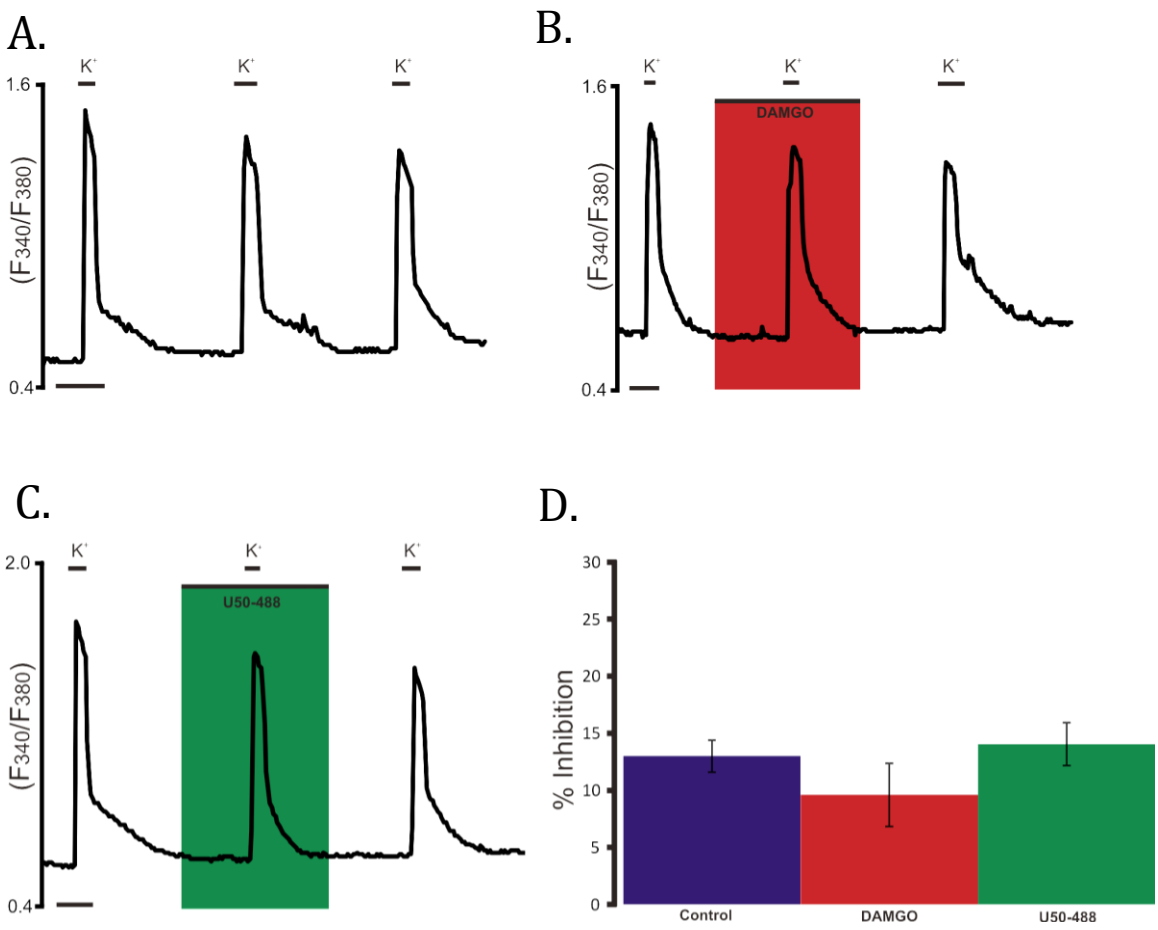

Effect of 10μM DAMGO

With concentrations of 1μM having no statistically significant effect on voltage-gated Ca^{2+} influx, the concentrations of the agonists were increased to 10μM. This is the maximal concentration that can be used to keep selectivity among the individual receptors. At a concentration of 10μM (Figure 14), DAMGO had an average percent inhibition of voltage-gated Ca^{2+} influx of 26.23 ± 2.92% (N=11). Compared to the controls, 10μM DAMGO had a statistically significant ($p<0.0004$) effect on the voltage-gated Ca^{2+} influx.

Effect of 10μM U50-488

At a concentration of 10μM, U50-488 elicited an average percent inhibition of voltage-gated Ca^{2+} influx of 22.22 ± 2.47% (N=11). Compared to the controls, 10μM U50-488 had a statistically significant ($p<0.003$) effect on the voltage-gated Ca^{2+} influx (Figure 14).

PERTUSSIS TOXIN

Pertussis toxin (PTX) was used as a G_i protein inhibitor to confirm the pathway hypothesized in this thesis (Mangmool & Kurose, 2011; Holz *et al*, 1986). PTX catalyzes the ADP-ribosylation of G proteins and by doing so prevents the agonist-induced dissociation of the proteins into active subunits (Katada *et al*, 1984; Holz *et al*, 1986). PTX-sensitive G proteins typically inhibit high-threshold Ca^{2+} channels of the N- and P/Q-types, of which P/Q-types are located on the CB (Buckler & Vaughan-Jones, 1994; Hille, 1994). Cells were incubated for 3 hours in the

presence of 150 ng/ml of PTX and Ca^{2+} imaging examined the effects on voltage-gated Ca^{2+} influx (Holz *et al*, 1986).

Figure 14. Effects of 10μM DAMGO and 10μM U50-488 on type I CB cell Fura-2 Fluorescence ratios. The control example cell (A) shows the slight decrease in 80mM K^+-evoked Ca^{2+} entry after repeated applications of K^+ over time (N=12). The example cell exposed to 10μM DAMGO (N=11), as seen by the red box (B), shows a statistically significant inhibition of 80mM K^+-evoked Ca^{2+} entry into the cell ($p<0.0004$). The experimental example cell exposed to 10μM U50-488 (N=8), as seen by the green box (C), shows a statistically significant inhibition of 80mM K^+-evoked Ca^{2+} entry into the cell ($p<0.003$). The histogram (D) shows the average percent inhibitions for the controls (12.99± 1.34%), 10μM DAMGO (26.43± 2.92%) and 10μM U50-488 (22.22 ± 2.47%). Scale bar indicates 2 minutes.

Figure 14.

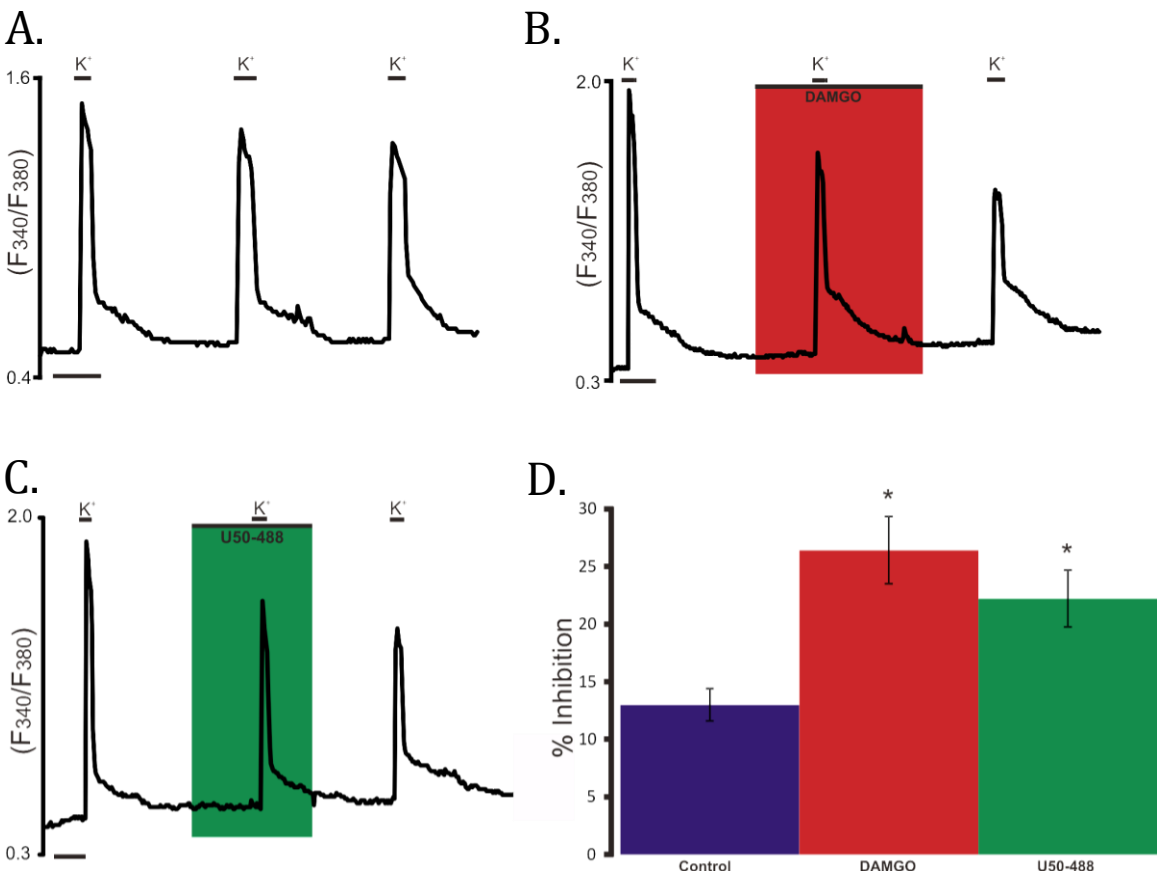

Controls in the presence of PTX

The first K^+ response was not statistically different from the first K^+ response of the controls that were not incubated with PTX ($p<0.53$). This was tested to ensure that PTX did not affect the Ca^{2+} handling properties or excitability of the type I CB cells. The controls after the incubation with PTX (N=7) had an average inhibition of 11.22 ± 2.66% (Figure 15).

Effect of 10μM DAMGO with PTX incubation

After incubating with PTX, the average inhibition of the voltage-gated Ca^{2+} influx by 10μM DAMGO (N=12) was 18.95 ± 3.02% (Figure 15). Compared to the controls also incubated with PTX, the effect of 10μM DAMGO on the response to K^+ was not statistically significant after a 3 hour incubation with 150 ng/ml of PTX ($p<0.1$).

Effect of 10μM U50-488 with PTX incubation

After incubating with PTX, the average inhibition of the voltage-gated Ca^{2+} influx by 10μM U50-488 (N=7) was 17.47 ± 1.81% (Figure 15). Compared to the controls also incubated with PTX, the effect of 10μM U50-488 on the response to K^+ was not statistically significant after a 3 hour incubation with 150 ng/ml of PTX ($p<0.08$).

Figure 15. Effects of 10μM DAMGO and 10μM U50-488 on type I CB cell Fura-2 Fluorescence ratios after a 3 hour incubation with PTX. All cells (including controls)

were treated with a 3 hour incubation in 150 ng/ml of PTX. The control example cell (A) shows the slight decrease (11.21 ± 2.66%) in 80mM K^+-evoked Ca^{2+} entry after repeated applications of K^+ over time (N=7). Neither the example cell exposed to 10μM DAMGO (N=12), as seen by the red box (B), nor the example cell exposed to 10μM U50-488 (N=7), as seen by the green box (C), show a statistically significant inhibition of 80mM K^+-evoked Ca^{2+} entry into the cell. The histogram (D) shows the average percent inhibitions for the controls (11.21 ± 2.66%) 10μM DAMGO (18.95 ± 3.02%) and 10μM U50-488 (17.47 ± 1.81%). Scale bar indicates 2 minutes.

Figure 15.

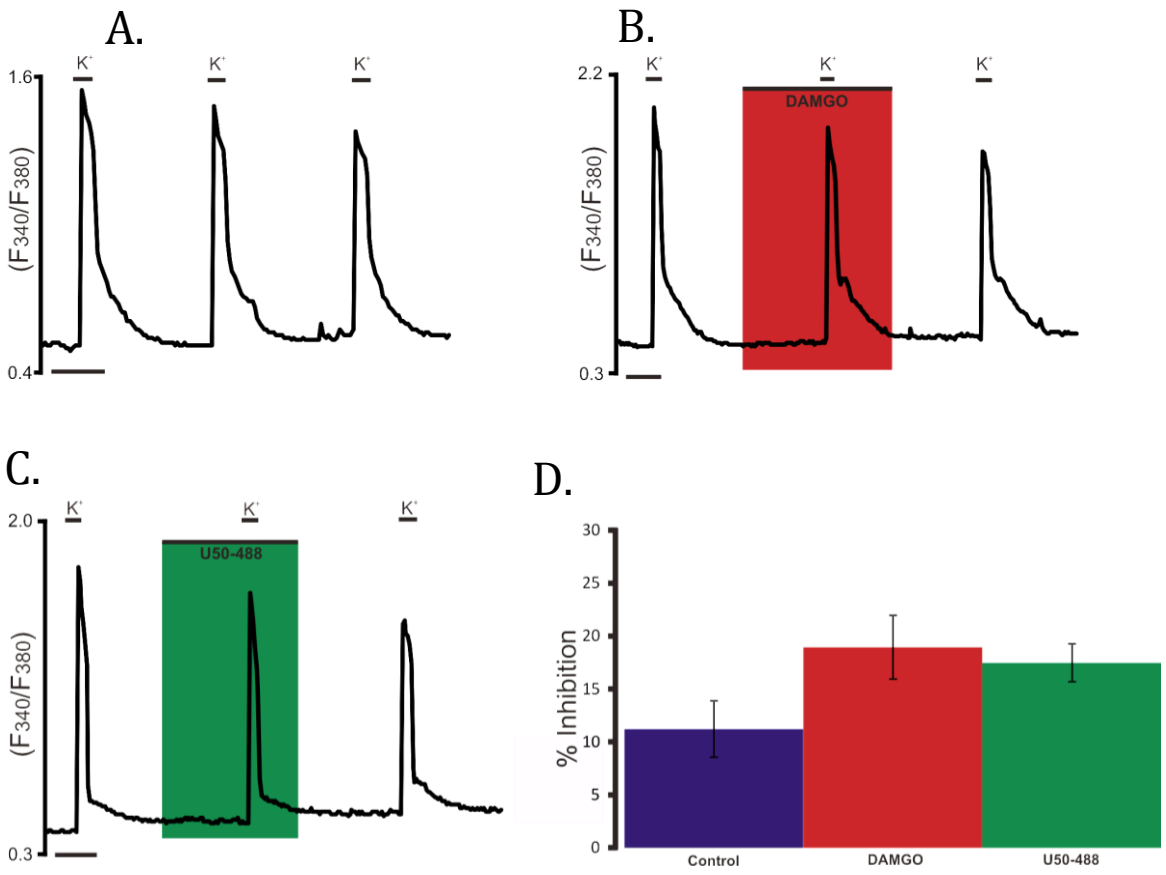

DISCUSSION

RESULTS SUMMARY

Through immunohistochemistry, it was discovered that μ and κ opioid receptors were present on the rat type I CB cells, whereas δ opioid receptors were not present. When tested, with their selective agonist at 1μM concentrations, both DAMGO for the μ opioid receptor, and U50-488 for the κ opioid receptor, were not statistically significant at inhibiting voltage-gated Ca^{2+} entry into the type I cell. However, at 10μM, DAMGO and U50-488 were both statistically significantly at inhibiting voltage-gated Ca^{2+} entry into the type I cell.

Following a 3 hour incubation in PTX, a G_i protein inhibitor, neither 10μM DAMGO nor 10μM U50-488 were statistically significant when it came to inhibiting voltage-gated Ca^{2+} entry into the type I cell. Therefore, it can be concluded that the

opioid receptor-mediated inhibition of voltage-gated Ca^{2+} influx occurs via PTX-sensitive G_i proteins.

These data support the hypothesis and show that when activated by agonists, the μ and κ opioid receptors on type I CB cells activate G_i proteins which inhibit the influx of voltage-gated Ca^{2+}, which could reduce neurotransmitter release, decreasing the firing rate to the CSN, and ultimately inhibiting the acute hypoxic response in the peripheral nervous system.

FUTURE EXPERIMENTS

Although it has been concluded that the inhibition occurs via a PTX-sensitive G_i protein pathway, the inhibition is relatively small when compared to the concentrations of the agonists applied. Since it is no longer possible to increase the concentrations of our agonists without losing selectivity to their receptors, it is probable that the G_i proteins are working through other pathways to decrease the neurotransmitter release and thereby decrease the firing rate of the CSN. The $G_{\beta\gamma}$ subunit binds to voltage-gated Ca^{2+} channels causing inhibition, but it has also been shown to directly bind to synaptic machinery (Figure 4) through a separate mechanism (Wells *et al*, 2012; Blackmer *et al*, 2005). By affecting the SNARES and SNAP proteins that enable the neurotransmitters to be released from the cell, the $G_{\beta\gamma}$ subunit could inhibit neurotransmitter release more directly and further inhibit the CSN firing leading to an inhibition of the acute hypoxic response.

To examine if opioid receptors are coupled to the exocytotic machinery, a future experiment could be to measure neurotransmitter release at a constant level

of intracellular calcium (Figure 16). Man-Song-Hing *et al* used a similar technique to measure neurotransmitter release while clamping Ca^{2+} at a constant level in *Helisoma* neurons (1989), but it could be challenging to replicate these techniques in type I cells due to the difficultly in measuring neurotransmitters released from isolated type I CB cells.

Additionally, the experiments presented in this thesis were completed on samples of both male and female rats and no analysis was done comparing the effects of agonists based on gender because our data did not seem to conform to two main groups. However, it would be interesting to perform more experiments comparing the effects of agonists on voltage-gated Ca^{2+} influx in males to the effects in females due to the fact that female rat brains were less sensitive than male rat brains to the effects of κ opioid receptor agonist U50-488 (Russell *et* al, 2013).

Figure 16. Schematic showing a possible future experiment to test whether $G_{\beta\gamma}$ subunits bind to synaptic machinery. To assess whether opioid receptors on type I CB cells are coupled to exocytotic machinery, intracellular calcium must be clamped at a constant level. This would allow the researcher to conclude that the $G_{\beta\gamma}$ subunit was not only affecting the voltage-gated Ca^{2+} channels, but that it also was involved in altering the neurotransmitter release directly which could drastically inhibit the acute hypoxic response in the peripheral nervous system.

Figure 16.

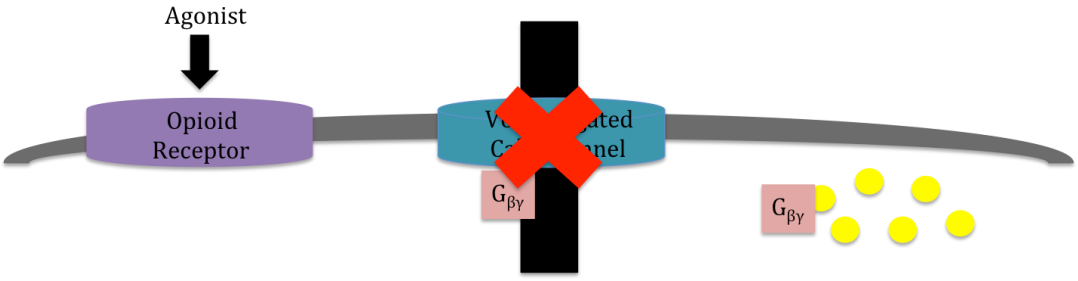

Another possible thought would be to explore if opioid receptors were in the endothelium of the blood vessels supplying the CB and if activation of these opioid receptors had an effect on the acute hypoxic response. However, using a reverse transcriptase polymerase chain reaction and Southern blotting, it was shown that opioid expression was not found in the endothelium of rats (Wittert *et al*, 1996).

CONCLUSIONS

Type I CB cells sense changes in blood gases and release neurotransmitters that cause hyperventilation to restore homeostasis. Opiates blunt this acute hypoxic response, which can result in irregular breathing patterns. The purpose of this work was to identify the mechanism by which opioids affect breathing in the peripheral nervous system through the CB. The results indicate that at concentrations of 10μM,

DAMGO and U50-488 inhibit voltage-gated Ca^{2+} influx into the type I cells. This inhibition could lead to a reduced release of neurotransmitters, a reduced firing of the CSN, and ultimately an inhibition of the acute hypoxic response in the peripheral nervous system. Although other mechanisms play into the inhibition of the acute hypoxic response, it can be concluded from this work that the inhibition of voltage-gated Ca^{2+} channels is a part of the overall effect.

REFERENCES

Al-Hasani, Ream., & Bruchas, M.R., 2011. Molecular mechanisms of opioid receptor-dependent signaling and behavior. *Anesthesiology* **115(6)**: 1363-1381.

Ballanyi, K., Panaitescu, B., Ruangkittisakul, A., 2010. Indirect opioid actions on inspiratory pre-Bötzinger complex neurons in newborn rat brainstem slices. *Adv. Exp. Med. Biol.* **669**: 75-79.

Blackmer, T., Larsen, E. C., Bartleson, C., Kowalchyk, J. A., Yoon, E., Preininger, A. M., Alford, S., Hamm, H. E., Martin, T. F. J., 2005. G protein βγ directly regulated SNARE protein fusion machinery for secretory granule exocytosis. *Nature Neurosci.* **8(4)**:421-425.

Buckler, K.J., 1997. A novel oxygen-sensing potassium channel in rat carotid body type I cells. *J. Physiol.* **498**: 649-662.

Buckler, K.J., & Vaughan-Jones, R.D., 1994. Effects of hypoxia on membrane potential and intracellular calcium in rat neonatal carotid body type I cells. *J. Physiol.* **3**:423-428.

Clark, J. A., & Pasternak, G. W., 1988. U50,488: a kappa-selective agent with poor affinity for mu1 opiate binding sites. *Neuropharm.* **27(3)**: 331-332.

Codd, E.E., Carson, J.R., Colburn, R.W., Stone, D.J., Van Besien, C.R., Zhang, S. P., Wade, P. R., Gallantine, E. L., Meert, T. F., Molino, L., Pullan, S., Rasler, C. M., Dax, S. L., Flores, C. M., 2009. JNJ-20788560 [9-(8-azabicyclo[3.2.1]oct-3-ylidene)-9H-xanthene-3-carboxylic acid diethylamide], a selective delta opioid receptor agonist, is a potent and efficacious antihyperalgesic agent that does not produce respiratory depression, pharmacologic tolerance, or physical dependence. *J Pharmacol Exp Ther* **329:** 241-51.

De Kock, L.L., & Dunn, A.E., 1966. An electron microscopic study of the carotid body. *Acta. Anatomica* **64**: 163-173.

Dayanithini, G., Stuenkel, E. L., Nordmann, J. J., 1992. Intracellular calcium and hormone release from nerve endings of the neurohypophysis in the presence of opioid agonists and antagonists. *Exp. Brain Res.* **90(3):** 539-545.

Dinger, B., Gonzalez, C., Yoshizaki, K., Fidone, S., 1981. [3H] Spiroperidol binding in normal and denervated carotid bodies. *Neurosci. Lett.* **1**: 51-55.

Docherty, R.J., McQueen, D.S., 1978. Inhibitory action of dopamine on cat carotid chemoreceptors. *J. Physiol.* **279**: 425-436.

Feng, Y., He, X., Yang, Y., Chao, D., Lazarus, L., Xia, Y., 2012. Current research on opioid receptor function. *Curr. Drug Targets* **13(2)**: 230-246.

Finley, J.C., & Katz, D.M., 1992. The central organization of carotid body afferent projections to the brainstem of the rat. *Brain Res.* **1-2**: 108-116.

Gerard, M.W, & Billingsly, P.R., 1923. The innervation of the carotid body. *Anat. Rec.* **26**: 391-400.

Gonzalez, C., Almaraz, L., Obeso, A., & Rigual, R., 1994. Carotid body chemoreceptors: from natural stimuli to sensory discharges. *Physiol. Rev.* **4**: 829-898.

Gonzalez, C., Lopez-Lopez, J.R., Obeso, A., Perez-Garcia., M.T., Rocher, A., 1995. Cellular Mechanisms of oxygen chemoreception in the carotid body. *Respir. Physiol.* **102**: 137-147.

Gonzalez-Guerrero, P.R., Rigual, R., Gonzalez, C., 1993a. Effects of chronic hypoxia on opioid peptide and catecholamine levels and on the release of dopamine in the rabbit carotid body. *J. Neurochem.* **60**: 1769-1776.

Gonzalez-Guerrero, P.R., Rigual, R., Gonzalez, C., 1993b. Opioid peptides in the rabbit carotid body: identification and evidence for co-utilization and interactions with dopamine. *J. Neurochem.* **60**: 1762-1768.

Greer, J. J., Carter, J. E., Al-Zubaidy, Z., 1995. Opioid depression of respiration in neonatal rats. *J. Physiol.* **485(3)**: 845-855.

Haji, A., & Takeda, R., 2001. Effects of a kappa-receptor agonist U50-488 on bulbar respiratory neurons and its antagonistic action against the mu receptor-induced respiratory depression in decerebrate cats. *Jpn. J. Pharmacol.* **87:** 333-337.

Han, J. N., Stegen, K., Cauberghs, M., Van de Voestijne, K. P., 1997. Influence of awareness of the recording of breathing on respiratory pattern in healthy humans. *Eur. Respir. J.* **10**: 161-166.

Handa, B. K., Lane, A. C., Lord, J. A. H., Morgan, B. A., Rance, M. J., Smith, C. F. C., 1981. Analogues of β-LPH_{61-64} possessing selective agonist activity at μ-opiate receptors. *Eur. J. Pharmacol.* **70:** 531-540.

Hille, B., 1994. Modulation of ion-channel function by G-protein-coupled receptors. *Trends Neurosci.* **17**: 869-875.

Holz, G. G., Rane, S. G., Dunlap, K., 1986. GTP-binding proteins mediate transmitter inhibition of voltage-dependent calcium channels. *Nature* **321(20)**: 670-672.

Inyushkin, A.N., 2007. Effects of leucine-enkephalin on potassium currents in neurons in the rat respiratory center in vitro. *Neurosci. Behav. Physiol.* **7**: 739-746.

Katada, T., Bokoch, G. M., Northup, J. K., Ui, M., Gilman, A. G., 1984. The inhibitory guanine nucleotide-binding regulatory component of adenylate cyclases. Properties and function of the purified protein. *J. Biol. Chem.* **259(6):** 3568-3577.

Kelly, E., 2013. Efficacy and ligand bias at the μ-opioid receptor. *Br. J. Pharac.* **169**: 1430-1446.

Kirby, G. C., & McQueen, D. S., 1986. Characterization of opioid receptors in the cat carotid body involved in chemosensory depression in vivo. *Br. J. Pharmac.* **88**: 889-898.

Kumar, P., & Prabhakar, N., 2012. Peripheral chemoreceptors: function and plasticity of the carotid body. *Compr. Physiol.* **2**: 141-219.

Lalley, P. M., 2003. Mu-opioid receptor agonist effects on medullary respiratory neurons in the cat: evidence for involvement in certain types of ventilatory disturbances. *Am. J. Physiol. Regul. Integr. Comp. Physiol.* **285:** 1287-1304.

Lazarov, N.E., Reindl, S., Fischer, F., Gratzl, M., 2009. Histaminergic and dopaminergic traits in the human carotid body. *Respir. Physiol. Neurobiol.* **165**: 131-136.

Lopez-Barneo, J., Lopez-Lopez, J.R., Urena, J., Gonzalez, C., 1988. Chemotransduction in the carotid body: K^+ current modulated by PO_2 in type I chemoreceptor cells. Science **241**: 580-582.

Lopez-Barneo, J., del Toro, R., Levitsky, KL., Chiara, MD., Ortega-Saenz, P., 2004. Regulation of oxygen sensing by ion channels. *J. Appl. Physiol.* **96**: 1187-1195.

Lord, J.A.H., Waterfield, A.A., Hughes, J., Kosterlitz, H.W., 1977. Endogenous opioid peptides: multiple agonists and receptors. *Nature* **267**: 495-499.

Man-Song-Hing, H., Zoran, M. J., Lukowiak, K., Haydon, P. G., 1989. A neuromodulator of synaptic transmission acts on the secretory apparatus as well as on ion channels. *Lett. Nature.* **341:** 237-239.

Mangmool, S., & Kurose, H., 2011. $G_{i/o}$ protein-dependent and –independent actions of pertussis toxin (PTX). *Toxins.* **3**: 884-899.

Mansour, A., & Watson, S. J., 1993. Anatomical distribution of opioid receptors in mammalians: an overview. *Hand. Exp. Pharmacol.* **104:** 79-105.

Martin, W.R., 1967. Opioid antagonists. *Pharmac. Rev.* **19**: 463-521.

Mayer, N., Zimpfer, M., Raberger, G., Beck, A., 1989. Fentanyl inhibits cancine carotid chemoreceptor reflex. *Anest.h Analg.* **69**: 756-762.

Mir, A.K., McQueen, D.S., Pallot, D.J., Nahorski, S.R., 1984. Direct biochemical and neuropharmacological identification of dopamine D2-receptors in the rabbit carotid body. *Brain Res.* **2**: 273-283.

Mutolo, D., Bongianni, F., Einum, J., Dubuc, R., Pantaleo, T., 2007. Opioid-induced depression in the lamprey respiratory network. *Neurosci.* **150:** 720-729.

Nurse, C.A., 1987. Localization of acetylcholinesterase in dissociated cell cultures of the carotid body in the rat. *Cell Tissue Res.* **250**: 21-27.

Pasternak, G.W., 2013. Opioids and their receptors: are we there yet? *Neuropharm.* **76B**: 198-203.

Pattinson, K. T. S., 2008. Opioids and the control of respiration. *Br. J. Anaesth*. **100**: 747-758.

Peers, C., Wyatt CN., Evans, M., 2010. Mechanisms for acute oxygen sensing in the carotid body. *Resp. Phys. Neuro.* **174**: 292-298.

Peers, C., 1990. Hypoxic suppression of K^+ currents in type-I carotid-body cells—selective effect on Ca^{2+}-activated K^+ current. *Neurosci. Lett.* **119**: 253-256.

Pradhan, A. A., Smith, M. L., Kieffer, B. L., Evans, C. J., 2012. Ligand-directed signaling within the opioid receptor family. *Br. J. Pharmacol.* **167:** 960-969.

Russell, S. E., Rachlin, A. B., Smith, K. L., Muschamp, J., Berry, L., Zhao, Z., Chartoff, E. H., 2013. Sex differences in sensitivity to the depressive-like effects of kappa opioid receptor agonist U50-488 in rats. *Biol. Phychiatry. In press.*

Satoh, M., & Minami, M., 1995. Molecular pharmacology of the opioid receptors. *Pharmac. Ther.* **68(3)**: 343-364.

Schweitzer, A., Wright, S., 1938. Action of prostigmine and acetylcholine on respiration. *Q. J. Exp. Phys.* **28**: 33-47.

Shirahata, M., Balbir, A., Otsubo, T., Fitzgerald, R.S., 2007. Role of acetylcholine in neurotransmission of the carotid body. *Resp. Phys. Neuro.* **157**: 93-105.

Teppema, L., & Dahan, A., 2010. The ventilator response to hypoxia in mammals: mechanisms, measurements, and analysis. *Physiol. Rev.* **90**: 675-754.

Vicario, I., Rigual, R., Obeso A., Gonzalez, C., 2000. Characterization of the synthesis and release of catecholamine in the rat carotid body in vitro. *Am. J. Physiol. Cell Physiol.* **278**: C490-C499.

Wakai, J., Kizaki, K., Yamaguchi-Yamada, M., Yamatoto, Y., 2010. Differences in tyrosine hydroxylase expression after short-term hypoxia, hypercapnia or hypercapnic hypoxia in rat carotid body. *Resp. Phys. Neuro.* **173**: 95-100.

Wang, Z., Bisgard., G.E., 2002. Chronic hypoxia-induced morphological and neurochemical changes in the carotid body. *Microsc. Res. Tech.* **59**: 168-177.

Wells, C. A., Betke, K. M., Lindsley, C. W., Hamm, H. E., 2011. Label-free detection of G protein—SNARE interactions and screening for small molecule modulators. *ACS Chem. Neuro.* **3**: 69-78.

Wittert, G., Hope, P., Pyle, D., 1996. Tissue distribution of opioid receptor gene expression in the rat. *Biomed. Biophys. Res. Comm.* **218:** 877-881.

Wyatt, C.N., Peers, C., 1993. Nicotinic acetylcholine receptors in isolated type I cells of the neonatal rat carotid body. *Neuroscience* **1**: 275-281.

Zhang, M., Zhong, H., Vollmer, C., Nurse, C.A., 2000. Co-release of ATP and ACh mediates hypoxic signaling at rat carotid body chemoreceptors. *J. Physiol.* **525**: 143-158.

Zhang, X., Bao, L., 2012. Interaction and regulatory functions of μ- and δ-opioid receptors in nociceptive afferent neurons. *Neurosci. Bull.* **28(2)**: 121-130.

Zhang, Z., Zhuang, J., Zhang, C., Xu, F., 2011. Activation of opioid μ-receptors in the commissural subdivision of the nucleus tractus solitarius abolishes the ventilatory response to hypoxia in anesthetized rats. *Anesthes.* **115(2)**: 353-363.